Experimental Study on Hydro-mechanical Behaviour of Rock Joints by using Parallel-Plates Model Containing Contact Area and Artificial Fractures

Bo LI[1)], Yujing JIANG[2), 3)], Tomofumi, KOYAMA[4)], Lanru JING[4)], Yoshihiko TANABASHI[2)]

[1)] Graduate School of Science and Technology, Nagasaki University, Nagasaki 852-8521, Japan

[2)] Faculty of Engineering, Nagasaki University, Nagasaki 852-8521, Japan

[3)] Research Center for Geo-environmental Science, Dalian University, Dalian 116622, P.R.China

[4)]Engineering Geology and Geophysics Research Group, Department of Land and Water Resources Engineering, Royal Institute of Technology, KTH, S-100 44 Stockholm, Sweden

ABSTRACT: In recent years, geological disposal of radioactive wastes is considered to be the most promising option, which requires the understanding of the coupled mechanical, hydraulic and thermal properties of the host rock masses and rock fractures. The hydro-mechanical behavior and properties of rock fractures are usually determined by laboratory experiments on fracture specimens that serve as the basic building block of the constitutive models of fractured rock masses.

Laboratory testing of rock fractures involve a number technical issues that may have significant impacts on the reliability and applicability of the testing results, chief among them are the quantitative estimation of the evolutions of hydraulic transmissivity fields of fractures during shear under different normal constraint conditions, and the sealing techniques when fluid flow during shear is involved. In this study, a new shear-flow testing apparatus with specially designed fluid sealing techniques for rock fractures were developed, under constant normal load (CNL) or constant normal stiffness (CNS) constraint. The topographical data of all fracture specimens were measured before testing to constitute the geometrical models for simulating the change of mechanical aperture distributions during shearing. A number of shear-flow coupling tests were carried out on three kinds of rock fracture specimens to evaluate the influence of morphological properties of rock fractures on their hydro-mechanical behaviour. Some empirical relations were proposed to evaluate the effects of contact area and surface roughness on the behavior of fluid flow through rock fractures.

Keywords: Hydromechanical; Rock fracuture; Coupled shear-flow test; Roughness; Transimissivity.

1. INTRODUCTION

In recent years, the development and utilizations of deep underground spaces like radioactive waste repositories have received great attention in international communities. The performance and safety of these facilities depends on the knowledge of permeability of rock masses, which varies with in situ and disturbed stresses around the repositories and the hydro-mechanical behaviors of rock fractures. Particularly for high-level radioactive waste disposal facilities in crystalline rocks, their safety assessments are mainly based on knowledge of paths and travel times of radioactive nuclide transport that is dominated by groundwater flow in rock fractures.

When rock fractures experience a relative displacement process, the void spaces between their opposite surfaces, namely their apertures, may increase (dilation) with relative shear or decrease (closure) with normal loads, respectively. A number of laboratory studies have been conducted to investigate the effect of normal loading on fluid flow through rock factures [1-7]. In recent years, the studies considering both the normal and shear stresses on fractures with fluid flow, the so-called coupled shear-flow tests, have attracted much attention [8-16]. It was found that fluid flows in a rock fracture through connected channels that bypassing the contacts areas [17]. However, the effects of contacts and the channel distribution patterns in a rock fracture undergoing both normal and shear displacements have not been fully understood, due mainly to the difficulties of quantitative representation of fracture surface roughness, and the limitations in flexible and reliable boundary conditions required for laboratory shear-flow tests. In addition, a number of empirical relations between mechanical and hydraulic apertures of rock fractures have been proposed such as by Barton et al. [12], whereas there still have not sufficient evidences, from either laboratory experiment or *in-situ*, to prove their validity in quantifying the fluid flows in coupled shear-flow system, besides the fact that a number of technical difficulties still exist in laboratory shear-flow testing, most notably the sealing of fluid during shear.

In laboratory shear testing, the constant normal loading (CNL) condition corresponds to the cases such as non-reinforced rock slopes, in concept. For deep underground opening or rock anchor-reinforced slopes, more representative behavior of rock fractures would correspond to a boundary condition of constant normal stiffness (CNS) [18]. One needs therefore to examine and understand the differences in the coupled shear-flow behaviors of rock fractures under these two boundary/loading conditions during laboratory experiments as the first step. To do this, however, requires clear conceptual understanding of possible rock fracture behaviours under these two conditions and efficient and reliable testing devices.

In the present study, a new laboratory test apparatus and its control system for coupled direct shear-flow tests under either CNL or CNS boundary conditions are reported. The

shear-flow coupling tests were carried out on three artificially created rock fracture specimens under various boundary conditions. Numerical models using the measured topographical data of fracture surfaces were conducted to simulate the change of void spaces and fluid flow during shearing. Finally, the relation between mechanical aperture and hydraulic aperture was discussed.

2. DESCRIPTION OF EXPERIMENT

2.1 Shear-flow test apparatus

Fluid flows through a rough fracture following connected channels bypassing the contact areas with tortuosity. These phenomena cannot be directly observed in ordinary laboratory tests without a visualization device. In this study, a laboratory visualization system of shear-flow tests under the CNS boundary condition is developed. The outline of the fundamental hardware configuration of this apparatus is described in Figure 1. It consists of the following five units:

(1) A hydraulic-servo actuator unit. This device consists essentially of two load jacks and two sets of linear-guides for applying uniform stresses on the upper and lower blocks of rock fracture specimens. Both normal and shear forces are applied by hydraulic cylinders through a servo-controlled hydraulic pump. The loading capacity is 100kN in both normal and shear directions. The shear force is applied on the specimen holder through two horizontal holding arms.

(2) An instrument package unit. This system contains two digital load cells for measuring shear and normal loads. Displacements are measured through two LVDTs (linear variation displacement transducers), in which the one for measuring shear displacement is attached between load cells and load jacks and the other one for measuring normal displacement is set between the upper and lower blocks of the specimen.

(3) A mounting shear plate unit. This unit consists of a lower and an upper plate. The upper plate connects to a slide guide that can only move in the horizontal direction. It ensures the minimum friction and bending movement when the upper shear box moves during shearing. The lower plate connects to another slide guide who can only move in the vertical direction and the specimen holder is set between these two plates.

(4) A water supplying, sealing and measurement unit. Constant water pressure is obtained from an air compressor connecting to a water vessel. The water pressure is controlled with a regulator ranging from 0 to 1 MPa. The two sides of specimen parallel to the shear direction are sealed with gel sheets, which are very flexible with perfect sealing effect and minimum effect to the mechanical behavior of the shear testing. The weight of water flowing out of the

fracture is measured by an electrical balance in real time.

(5) A visualization unit. When acrylic transparent replicas of rock fractures with natural surface features are used as the upper block of a fracture specimen in tests, the images of the fluid flow in the fractures are captured by a CCD camera through a observation hole on the upper shear plate. Colored water can be used to enhance the visibility of the flow paths.

The CNS boundary condition is reproduced by a closed-loop in the system control software, with electrical and hydraulic servo-controls. A nonlinear feedback of control and measurement are carried out on a PC window through a multifunction analog-to-digital, digital-to-analog and digital input/output (A/D, D/A and DIO) board. Collected test data include the normal and shear forces, corresponding displacements and the strokes of the vertical and horizontal loading cylinders. The digital control program was designed by using the LabVIEW programming language [18].

2.2 Fracture surface measuring system

To obtain the topographical data of rock fracture surfaces, a three-dimensional laser scanning profilometer system with an accuracy of ±20 μm and a resolution of 10 μm, was employed. A X-Y positioning table is added to the laser scanner, which can move automatically by pre-programmed paths, together with a PC performing data collecting and processing in real time. All surfaces of rock fracture specimens were measured with an interval of 0.2mm in both x and y-axis in this study.

2.3 Fracture sample preparation

Two cuboid acrylic resin blocks with circular hard plastic shells were used to test the effects of contact areas on fluid flow, which is described in section 3.

Three rock fracture specimens, labeled as J1, J2 and J3, were taken from the construction site of Omaru power plant in Miyazaki prefecture in Japan, and were used as prototypes to producing artificial replicas of rock fractures [19], which were used in the coupled shear-flow test as mentioned in section 4. The specimens (replicas) are 100mm in width, 200mm in length and 100mm in height, and were made of mixtures of plaster, water and retardant with weight ratios of 1: 0.2: 0.005. The surfaces of the natural rock fractures were firstly re-cast by using the resin material, then the two parts of a specimen were manufactured based on the resin replica. The figure models constituted from the scanning data of the rock replicas re-cast from the same resin model are well matched even to the small asperities in a scale of 0.2mm. Therefore, the two parts of each specimens used in this study are almost perfectly mated. Table 1 shows the physical properties of these rock-like specimens.

3. TESTS ON PARALLEL-PLATE MODELS WITH VARYING CONTACT AREAS

3.1 Test procedure

A rock fracture contains asperities where the two surfaces of the fracture are in contact. Surrounding these asperities in contacts are the open regions defining the aperture h that may vary from point to point [17]. The parallel plate model following a cubic law for fluid flow is commonly adopted for fluid conductivities of rock fractures. This model, however, may or may not be universally valid under any conditions and its properties depend much on the distribution of the contact areas and hydraulic gradients. To evaluate the effects of contacts on the fluid flow through a fracture, in this study, a simple artificial parallel-plate model was used in hydraulic tests by changing the arrangement and ratio of contact areas. The model was constituted by two cuboid acrylic resin blocks with high modulus of elasticity so that a fracture with uniformly shaped and regularly distributed asperities on the fracture walls could be created to simplify the testing and analysis.

Assuming that contact spots on fracture surfaces are formed by asperities of circular cross-sections and defining a contact ratio c representing the ratio of total area of contact spots over the apparent area of the whole fracture specimen, we found, from a similar previous study [20], that the value of c of rock fractures is usually less than 0.3. A value of c equal to 0.25 was reported in [21]. For a sensitivity analysis, we tested three sets of artificial fracture specimens with contact ratio c equal to 0.15, 0.2 and 0.25, respectively, and each set has three geometrical arrangement patterns of contact spots (Fig.2). A fracture specimen with c= 0.3 was tested with only one geometrical arrangement pattern, as a supplement.

A kind of circular hard plastic shell was used to simulate asperities of circular shapes with known stiffness, heights and areas of cross sections as contacts. Its heights and modulus of elasticity were carefully measured so that the heights of contacts representing the mechanical aperture can be determined precisely under any known normal stress. We tested the artificial fracture specimens with apertures of 0.07mm, 0.14mm, 0.21mm, 0.28mm and 0.35mm for each geometrical arrangement of contact spots with hydraulic gradients of 0.5, 2.5, 5 and 10 (0.0001-0.002MPa in hydraulic pressure), respectively. The flow rates of each test case were measured and their transmissivities were evaluated by using the cubic law as follows:

$$Q = \frac{g}{\nu}\frac{we^3}{12}i \tag{1}$$

where g is the acceleration due to gravity, e is the hydraulic aperture, ν is the kinematic viscosity, w is the width of the flowing zone between the parallel plates.

3.2 Test results

The measured transmissivity values corresponding to specimens of contact ratios 0.15, 0.2 and 0.25 with different geometrical arrangement patterns of contact spots are shown in Figure 2. The measured values do not strictly follow the theoretical curve of the cubic law without any contact spot and the difference increases with increasing values of aperture. The impact of the different geometrical patterns of contact spots is, on the other hand, not so significant for the specimens used in our study when the overall contact ratio is kept the same. Comparing the differences in transmissivities of the specimens with different contact ratios, it shows that the larger the value of c is, the larger the discrepancies between the measured data and the theoretical curve of the cubic law.

Evaluation of the effect of contact area on the permeability of rock fractures has been reported in literatures by the numerical simulations or experiments [17, 22]. In [22] it was proposed that for potential flow around a single circular obstruction, the following equation describing relations between hydraulic aperture and contact ratio can be written as

$$h_H^3 = h_0^3 \frac{1-c}{1+c} \tag{2}$$

where $h_H{}^3$ is the hydraulic conductance with aperture h_H and h_0 is the effective aperture, respectively. This expression was validated numerically in [17] for contact ratio (circular asperity contact spot concentrations) up to 0.25. By using the effective medium theory, another form of the prediction was proposed in [23]

$$h_H^3 = h_0^3(1-2c) \tag{3}$$

For the experiments using plastic contact simulators as presented above in this study, the hydraulic conductance $h_H{}^3$ versus the cube of effective hydraulic aperture $h_0{}^3$ for contact ratio 0.15 is illustrated in Figure 3. Here, the effective hydraulic aperture is the width of aperture in the opening area, distinguishing with the mechanical aperture h_M or $\langle h \rangle$, which is the mean distance between two opposite surfaces of a fracture. The fluid flow is assumed to be governed by the cubic law. The hydraulic conductance is supposed to be constant at any hydraulic gradient when flow is laminar and steady. However, at $h_0{}^3$=42.9$\times 10^{-12}$m^3 in this figure, the hydraulic conductance drops its value with higher hydraulic gradient of 10. The flow rate is large and turbulent flow may have been developed and caused reduction of the

hydraulic conductance. The results in Figure 4 and later ones (Figure 7, 8 and 9) were calculated based on the lowest or the mean of the lowest two hydraulic gradients, in the condition of which, the fluid flow is thought to be steady and laminar. Decrease of conductance is one of the consequences of possible turbulent flow. The occurrence of turbulent flow needs to be confirmed by direct observation that will be reported later in a continued study.

3.3 Effect of contact area on fluid flow

The two equations (1) and (2) agree with each other at low concentrations of circular asperity contacts. Although they have been examined by numerical analysis, their validities still need to be affirmed by real hydraulic tests. We compared our experiment results to the predicted values by using these two equations as shown in Figure 4. The experimental data are located between the curves of these two equations, and fit more closely to equation (2). On the other hand, it should be noted that the accuracy of measurement is subjective to many factors for hydraulic testing of fracture specimens with apertures less than 1mm. An error of 0.1mm of h_0 could bring remarkable deviation from prediction values. Nevertheless, the experimental results proved that the tortuosity factor $1-\alpha c$ ($1<\alpha<=2$) used in these two equations could give reasonable prediction to the effect of circular contact areas on the transmissivity of fluid flow through a fracture. The decreased ratio of transmissivity due to the contact areas is generally greater than the ratio of contact areas itself. Therefore, herein α is an enlargement parameter to sufficiently quantify the effect of contact areas.

The total perimeter of contact spots is another factor affecting the transmissivity. We compared the hydraulic test results from two patterns of contact spots with the same contact ratio but different perimeters, and found that the pattern with smaller perimeter has higher transmissivity. Due to ‘no-slip’ conditions, the velocity vector of fluid must equal to zero at any boundaries of contact spots on a fracture surface, and the total perimeter of contacts could be used to quantify such boundaries. The longer the perimeter is, the larger “friction effect” the solids would bring to the fluid, thus decreasing the transmissivity. Only circular contact spot patterns were tested in this study, the real contact areas in a natural rock fracture, however, has different shapes, which obviously has significant effect on the transmissivity and will be examined in future.

4. SHEAR-FLOW COUPLING TEST ON ARTIFICIAL ROCK FRACTURES

4.1 Test procedure

Three natural rock fracture surfaces (as labeled J1, J2 and J3, respectively) were used as parent surfaces in this study as shown in Figure 5, based on which, three pairs of artificial fracture specimens were manufactured from each of these three natural fracture surfaces. These artificial fracture specimens are fully mated at the initial condition with contact ratio very close to 1.0. Among these fracture specimens, J1 is flat with very few major asperities on its surface. The surface of J2 is smooth but a major asperity exists at the center, and a few other large asperities on other locations. J3 is very rough with no major asperities but plenty of small ones. Test cases and their corresponding boundary conditions are shown in Table 2. In all of the tests, the flow direction is parallel to the shear direction and the cubic law was used to evaluate the transmissivities based on the measured flow rates. As the shearing goes on, the effective shear length (the length of the upper and lower parts of specimen facing to each other) will decrease, thus increasing the hydraulic gradient when the water head keeps constant. This effect has been considered in calculation of the transmissivity by decreasing the hydraulic gradient corresponding to the shear displacement. Topographical data of these rock fractures were also measured before testing to build the numerical simulation models.

Cyclic normal loading-unloading tests were firstly carried out before shear-flow coupling tests to obtain the maximum possible closures, based on which the mechanical apertures of fractures under a normal stress is calculated, using the data from the fourth cycle. By doing so, the normal stress-normal displacement curves could be obtained. Based on the hyperbolic function proposed by Bandis et al. [24], for simplifying the calculation, these curves can then be represented by the following equation.

$$\sigma = \alpha + \frac{\beta}{v + \delta_m} \tag{4}$$

where α and β are parameters deduced from the hyperbola curve, v is the normal displacement in experiment, σ is the normal stress and δ_m is the maximum possible closure of the fracture specimen.

The initial mechanical aperture E_0 is decided by the following equation:

$$E_0 = \delta_m - v_i \tag{5}$$

where v_i is the normal displacement corresponding to the initial normal load.

Cyclic loading tests have been carried out on the specimen with a fracture and the specimen with the same dimension and property but without fracture to determine their loading-deformation behaviors respectively. The difference of these two loading-displacement curves is the real deformation generated by the fracture. By doing so, the change of aperture

width under different loadings could be evaluated in the shear tests.

4.2 Test results

The shear behaviors of the tested fracture specimens are illustrated in Figure 6. For a fracture, larger shear stresses could be obtained under either higher normal stress or higher normal stiffness at the same initial normal stress, depending on the surface roughness and stiffness of asperities. Normal displacement is the most important behavior in the coupled shear-flow tests for quantifying the change of transmissivity. Normal displacement is usually called dilation because it is primarily an increasing process during a shearing. As shown in the figure, for a fracture specimen, the larger normal stress or normal stiffness is, the larger magnitude of normal displacement could be inhibited. Normal behavior of a fracture depends also on the roughness of the fracture surface. Generally, the rougher the fracture surface is, the larger normal displacement could be obtained [18, 20, 25].

As shown in Figure 7, the changes of transmissivities exhibit an obvious two-phase behavior. For all test cases, the transmissivities increase gradually in a relatively high gradient in the first several millimeters of shear displacement and then continue to increase but with a lower gradient gradually reaching to zero. Similar behaviors have also been reported in other shear-flow tests [8, 12]. The experimental results indicate that a rougher fracture may have higher gradient in the first phase and the second phase comes sooner. Under the same stress environment, a rougher fracture would produce larger normal displacement during shear so that it could obtain higher transmissivities in the second phase. The peak shear stress generally comes earlier than the turning point of transmissivity as shown in Figure 6 and Figure 7, which could be explained by the damage process of asperities on the fracture walls during shear as described in the next section. The Re numbers increase from almost 0 to as high as 1000 (depend on the hydraulic gradients) during the shear as the increase of flow rate. To avoid the occurrence of turbulent components in the fluid flow, the hydraulic gradients were carefully controlled to keep the Re numbers in an empirical range for laminar flow on the current test apparatus. The hydraulic gradients used in the shear-flow tests are in a range of 0.25-10 and they were decreased during the shear to inhibit the fast increases of flow rate and Re number. The maximum Re numbers (obtained from the last few minimeters of shear displacement) of the hydraulic data used for calculating the transmissivities of J1, J2 and J3 are 229, 240.6 and 225, respectively. Further improvement of the test apparatus supporting lower hydraulic gradients to avoid the turbulent flow without decreasing the accuracy of measurement is under construction.

4.3 Change of aperture during shearing

The changes of aperture distributions corresponding to the shear-flow coupling tests were simulated based on the measured topographical data. Mechanical apertures can be assessed based on the following equation [8]:

$$E_m = E_0 - \Delta E_n + \Delta E_s \tag{6}$$

where E_0 is the initial mechanical aperture, ΔE_n is the change of mechanical aperture by normal loading, and ΔE_s is the change of mechanical aperture by shearing. By using the normal stress-normal displacement curves in Section 4.1, the initial mechanical aperture E_0 under a certain normal stress can be obtained. Under the CNL boundary condition, ΔE_n could be taken as a constant, and ΔE_s is the measured normal displacement during shearing. For the test under the CNS boundary condition, the normal stress changes with the normal displacement, therefore, ΔE_n itself should be revised due to the corresponding normal stress during shearing and ΔE_s is also the measured normal displacement.

In the present study, the surfaces of fracture specimen were scanned with an interval of 0.2mm in *x* and *y*-axes, and the mechanical aperture under the CNL boundary condition at any point (*i*, *j*), where *i* is parallel to the shear direction and *j* is perpendicular to the shear direction at shear displacement *u* could be written as:

$$E_m(i,j) = E_0(i,j) + E_s(i,j) = E_0(i,j) + [V(u) + Z_L(i+u,j)] - Z_L(i,j) = Z_U(i+u,j) - Z_L(i,j) \tag{7}$$

where $V(u)$ is the normal displacement (dilation) at a shear displacement of *u* intervals, $i+u$ indicates the point number of the upper surface that directly mate with the current point *i* at the lower surface. Z_U and Z_L represent the heights of the upper and lower surfaces of the fracture specimen at any points from the lowest point of the lower surface, respectively.

Equation (7) is valid when the following conditions could be satisfied: (1) normal displacement totally contributes to the dilation of the mechanical aperture, (2) the deformation or damage of asperities could be neglected, (3) gouge materials developed during shearing have negligible influence on the fluid flow. Obviously, these conditions cannot be generally satisfied and the method used here therefore is a simplified one. For a parallel-plate model, dilation could be considered to contribute totally to the increase of the mechanical aperture. For a rough fracture, however, the contact, deformation and destruction of asperities would make structures of a fracture more complicated. Caution should be paid when using Equation (7) to evaluate the mechanical aperture during shearing since it is only a geometrical model.

Figure 8 shows the changes of aperture distributions of testing cases J1-1, J2-1 and J3-1

during shearing, respectively. The aperture fields change remarkably when a shear starts, i.e. in phase Ⅰ. After that, the change trends to become smaller and steady, due to the graduate reduction of dilation gradient as shown in Fig.6 in phase Ⅱ. The contact ratio changes reversely to the transmissivity change in a shearing, which represents an opposite effect of contact area on the transmissivity. There is a rapid drop of contact ratio in phase Ⅰ and then it keeps a small value in phase Ⅱ. For a rougher fracture, such reduction of contact ratio will be more significant. The peak shear stress occurs when the major asperities on the fracture surface lose their resistance to the shear and being destructed, while most asperities are undamaged and few gouge materials are generated. After that, the remaining asperities are crushed gradually, generating plenty of gouge materials and increasing the contact ratio. Therefore, the turning point of contact ratio occurs at almost the same time with that of the transmissivity and the effect of contact areas on the transmissivity of rock fracture is confirmed, which is also the basis of carrying out the study on parallel-plates model in Section 3.

The influences of morphological behaviors of rock fractures on the evolution of aperture distributions are also reflected in Figure 8. The surface of specimen J1 is smooth and flat. Therefore, its contact ratio is relatively high and its apertures distribute evenly over the fracture specimen. The few large asperities on the two parts of specimen J2 tended to climb over each other during shear, which decreased the contact ratio significantly and produced a large void space after a section of shear displacement (see the third figure in Figure 8 (b)). For specimen J3, the widely distributed asperities developed a complicated void space geometry, which causes complex structure of transmissivity field (Fig.8(c)).

4.4 Relation between mechanical aperture and hydraulic aperture

Zimmerman et al. [23] revealed that, in general, reasonably accurate predictions of conductivity could be made by combining either the perturbation results, Equation (7), or the geometric mean, Equation (8), with the tortuosity factor given by Equation (3), written as

$$h_H^3 \approx \langle h \rangle^3 [1 - 1.5\sigma_h^2 / \langle h \rangle^2 + \cdots] \tag{8}$$

$$h_H^3 = k_{eff} \approx k_G = e^{\langle \ln k \rangle} = e^{\langle \ln(h^3) \rangle} = e^{3\langle \ln k \rangle} = (e^{\langle \ln h \rangle})^3 = h_G^3 \tag{9}$$

where h_H is the hydraulic aperture, $\langle h \rangle$ is the arithmetic mean value of h, σ_h is the standard deviation of h, k_{eff} is the overall effective transmissivity, k_G is the geometric mean of the transmissivity distribution, and c is the contact ratio, respectively.

In this study, a series of combinations of different forms of aperture predictors with the tortuosity factor (1-2c) were evaluated as follows:

- Predictor (1): $\langle h^3 \rangle (1-2c)$
- Predictor (2): $\langle h \rangle^3 (1-2c)$
- Predictor (3): $h_G^3 (1-2c)$
- Predictor (4): $\langle h \rangle^3 [1-1.5\sigma_h^2 / \langle h \rangle^2](1-2c)$

Results are shown in Figure 9 for the tests on three kinds of fracture specimens under the CNL (σ_n=1MPa) boundary conditions, respectively. Herein, the "transmissivity " is not the ordinary T, but the cubic of mechanical aperture with a unit of 10^{-12} m^3. The results show that $\langle h \rangle^3$ is a more accurate predictor than $\langle h^3 \rangle$ for predicting hydraulic transmissivity. For the test case of J1-1, the mechanical aperture $\langle h \rangle$ itself agrees well with the hydraulic aperture h_H as back-calculated using the cubic law. Further modifications such as presented by predictor (3) or predictor (4) would underestimate the transmissivity. When the roughness of fracture increases, the predictors (3) and (4) give the closer predictions to the experiment data. For the test case of J3-1, the hydraulic aperture is much lower than the mechanical aperture, due to the influence of tortuosity produced by the complicated structure of void space and contact area. The tortuosity factor (1-2c) plays a significant role when combined with predictor (2) in Fig.9 (a) and (b), and with predictor (4) in Fig.9 (c). These predictors behave similarly for the other 6 test cases.

CONCLUSIONS

Two issues should be clarified when evaluating the hydro-mechanical behavior of a rock fracture undergoing shearing. The first one is the coupling between the shear behavior (shear stress and shear displacement) and normal behavior (normal stress, normal stiffness and normal displacement) for a rock fracture undergoing shearing. The normal stress and normal stiffness are generally set as boundary conditions. Together with shear displacement, they are applied to estimate the shear stress and normal displacement in laboratory or in situ tests, or to interpret shear process happening in natural rock masses. A number of models have been proposed to quantify this coupling mechanism, among which, the models given by Patton [26] and Barton [27] are generally accepted by engineers and scientists since they could give good prediction to the shear-normal behavior of natural rock fractures. More precise prediction is expected by developing more effective parameters to describe the surface roughness characteristics of rock fractures, and the models involving CNS boundary condition are also required.

The second issue is the coupling between the normal displacement and hydraulic conductivity, or the relation between the mechanical and hydraulic apertures. Cubic law could quantify the hydraulic behavior of most rock fractures. However, the existence of contact areas and channeling flow due to the tortuous connections of void spaces would bring deviations to its prediction. Two main considerations related to this problem are to modify the classical cubic law by introducing a "friction" factor *f* or to modify the relation between mechanical aperture and hydraulic aperture. Both of these two methods try to quantify how much the roughness on fracture surface affects the fluid flow through a fracture.

These two issues are not isolated but linked with each other by the normal behavior of a fracture in a coupled shear-flow test. The parameters to describe the roughness of fracture surface quantitatively and uniquely are needed for solving the problems raised by these two issues. In order to address these two issues in an more integrated and objective way, in this study, hydraulic tests on parallel-plate models with various contact ratios were conducted, together with replicas of rock fractures with three types of surface roughness features, leading to 9 coupled shear-flow tests under various CNL or CNS boundary conditions. The topographical data of specimens before testing were measured to develop the surface geometry models, which were used for simulating the changes of void spaces and contact areas during shearing.

The test results show that the tortuosity factor $1-\alpha c$ ($1<\alpha<=2$) can be used for characterizing the circular contacts. More accurate prediction of α values requires precision improvement of the test apparatus. For ellipse or more complicated contact spot shapes, α may have higher values, which needs to be examined in further experimental study. There is a two-phase behavior of both transmissivity and contact ratio *c* during shear. The transmissivity increases quickly in phase I until a threshold, after that, the gradient of transmissivity trends to 0. The "negative dilation" when a shear starts may deviate the transmissivity in phase I from the cubic law. Since mated fracture specimens were used in this study, the negative dilation herein originates from the contraction due to the consolidation of specimens under normal loading before shear. It could be considered as a special and fugacious phenomenon, during which the transmissivity is extremely low and its lowest value also could be used as the starting point of phase I to keep the gradient constant. Comparing to a flat fracture, a rough fracture could obtain higher value of transmissivity in phase Ⅱ and the threshold of phase I would come earlier. Higher normal stress or normal stiffness will inhibit the dilation of a rock fracture during shearing, thus decreasing the residual transmissivity in phase Ⅱ. The change of contact ratio in a shearing is just opposite to that of transmissivity.

Accurate prediction could be obtained by using the cubic law for relatively flat fractures, for which, the perturbation results, Equation (7) or the geometric mean, Equation (8) underestimates the transmissivity. As the fracture becomes rougher, the perturbation results or

the geometric mean provides closer approximations to the experimental results. Therefore, a standard is required to judge how rough a fracture is, the cubic law performs reasonably well without need for any modification. Dispersedly distributed contact areas could remarkably decrease the threshold for the validity of cubic law. Accurate prediction to the transmissivity in turbulent flow remains unsolved.

More shapes and distribution patterns of contact areas will be tested based on the parallel-plate model in the future study as well as improving the precision of the test apparatus. Shear-flow tests with flow direction perpendicular to that of shear direction is planned. Visual tracer test will be developed to find out more detailed information of the fluid flow though a rock fracture.

ACKNOWLEDGEMENTS

The authors wish to thank Mr. R. Saho and Mr. Y. Tasaku at Nagasaki University, for their experimental assistance throughout this study. This study has been partially funded by the Ministry of Education, Japan, Grant-in-Aid for Scientific Research (B), Research Project Number 11555131 and the National Natural Science Foundation of China (No. 50028403).

REFERENCE

[1] Detournay E. Hydraulic conductivity of closed rock fracture: an experimental and analytical study. In: Proc 13th Canadian Rock Mech Symp, 1980, pp 168-173.

[2] Durham WB, Bonner BP. Self-propping and fluid flow in slightly offset joints at high effective pressures. J Geophys Res 1994;99:9391-9399.

[3] Iwai K. Fundamental studies of fluid flow though a single fracture. PhD thesis, Univ Calif Berkeley, USA, 1976.

[4] Iwano. Hydromechanical characteristics of a single rock joint. PhD thesis, Massachusetts Institute of Technology, USA, 1995.

[5] Pyrak-Nolte LJ, Nolte DD, Myer LR, Cook NGW. Fluid flow through single fractures. In: Proc Int Symp Rock Joints, N Barton and O Stephansson. Balkema, eds. Rotterdam, 1990, pp 405-412.

[6] Raven KG, Gale JE. Water flow in a natural rock fracture as a function of stress and sample size. Int J Rock Mech Min Sci & Geomech Abstr 1985;22:251-261.

[7] Sundaram PN, Watkins DJ, Ralph WE. Laboratory investigations of coupled stress-deformation-hydraulic flow in a natural rock fracture. In: Proc 28th U. S. Symp Rock Mech, I Farmer, J Daemen, C Desai, C Glass, S Neuman, eds. Balkema, Rotterdam, 1995, pp 441-446.

[8] Esaki T, Du S, Mitani Y, Ikusada K, Jing L. Development of a shear-flow test apparatus and determination of coupled properties for a single rock joint. Int J Rock Mech Min Sci

1999;36:641-650.
[9] Gentier S, Lamontagne E, Archambault G, Riss J. Anisotropy of flow in fracture undergoing shear and its relationship to the direction of shearing and injection pressure, Int J Rock Mech Min Sci & Geomech Abstr 1997;34:3-4.
[10] Jiang Y, Tanabashi Y, Nagaie K, Li B, Xiao J. Relaitonship between surface fractal characteristic and hydro-mechanical behaviour of rock joints. In: Contribution of Rock mechanics to the New Century, Proc 3rd Asian Rock Mech Symp, Ohnishi Y, Aoki K, eds. Millpress, Rotterdam, 2004, pp 831-836.
[11] Makurat A, Barton N, Rad NS, Bandis S. Joint conductivity variation due to normal and shear deformation. In: Proc Int Symp Rock Joints, N Barton, O Stephansson, eds. Balkema, Rotterdam, 1990, pp 535-540.
[12] Olsson R, Barton N. An improved model for hydromechanical coupling during shearing of rock joints. Int J Rock Mech Min Sci & Geomech Abstr 2001;38:317-329.
[13] Olsson WA, Brown SR. Hydromechanical response of a fracture undergoing compression and shear. Int J Rock mech Min Sci & Geomech Abstr 1993;30:845-851.
[14] Lee HS, Cho TF. Hydraulic characteristics of rough fractures in linear flow under normal and shear load. Rock Mech Rock Eng 2002;35:299-318.
[15] Hans J, Boulon M. A new device for investigating the hydro-mechanical properties of rock joints. Int J Numer Anal Meth Geomech 2003;27:513-548.
[16] Auradou H, Drazer G, Hulin JP, Koplik J. Permeability anisotropy introduced by the shear displacement of rough fracture walls. Water Resour Res 2005;41:W09423,doi:10.1029/2005WR003938.
[17] Zimmerman RW, Chen DW, Cook NGW. The effect of contact area on the permeability of fractures. J Hydrology 1992;139:79-96.
[18] Jiang Y, Xiao J, Tanabashi Y, Mizokami T. Development of an Automated Servo-Controlled Direct Shear Apparatus Applying a Constant Normal Stiffness Condition. Int J Rock Mech Min Sci 2004;41:275-286.
[19] Jiang Y, Tanabashi Y, Nagaie K, Yamashita Y, Andou I. Stability Analysis for Underground Pumped Powerhouse Cavern in Jointed Rock Mass. In: Proc of the 11th International Conference of IACMAG2005, Torino, 2005, pp 671-677.
[20] Jiang YJ, Li B, Tanabashi Y. Estimating the relation between surface roughness an mechanical properties of rock joints. Int J Rock Mech Min Sci 2006;43:837-846.
[21] Witherspoon PA, Wang JSY, Iwai K, Gale JE. Validity of cubic law for fluid flow in a deformation rock fracture. Water Resour Res 1980;16:1016-1024.
[22] Walsh JB. The effect of pore pressure and confining pressure on fracture permeability. Int J Rock Mech 1981;18:429-435.
[23] Zimmerman RW, Bodvarsson GS. Hydraulic conductivity of rock fractures. Transport in

Porous Media 1996;23:1-30.
[24] Bandis SC, Lumsden AC, Barton NR. Fundamental of rock joint deformation. Int J Rock Mech 1983;20:249-268.
[25] Gentier SS, Riss J, Archambault G, Flamand R, Hopkins DL. Influence of fracture geometry on sheared behavior. Int J Rock Mech Min Sci 2000;37:161-174.
[26] Patton FD. Multiple modes of shear failure in rock. In: First Int Cong Rock Mech, Int Soc Rock Mech, Lisbon, 1966, pp 509-513.
[27] Barton N. Review of a new shear strength criterion for rock joints. Eng Geol 1973;7:287-332.

(a)

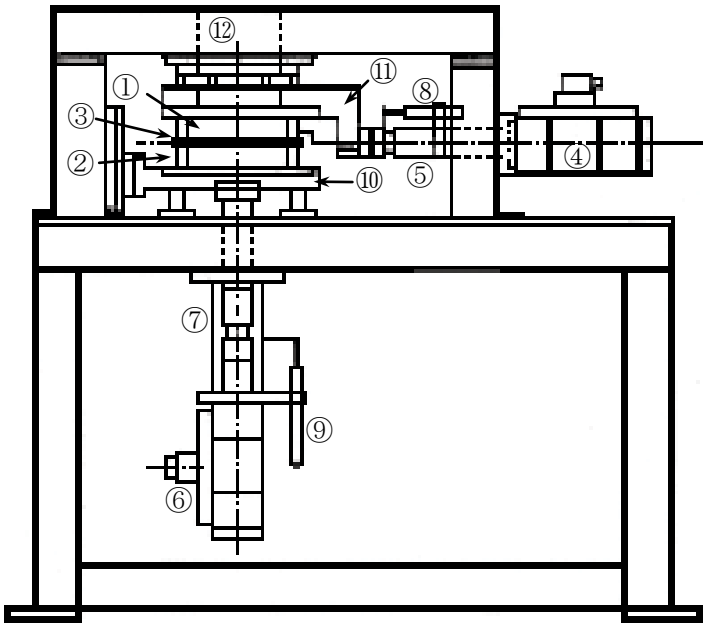

①: Specimen (upper part)
②: Specimen (lower part)
③: Gel sheet
④: Shear load jack
⑤: Shear load cell
⑥: Normal load jack
⑦: Normal load cell
⑧: LVDT (shear)
⑨: LVDT (normal)
⑩: Normal load plate
⑪: Shear load plate
⑫: Hole for visualization

(b)

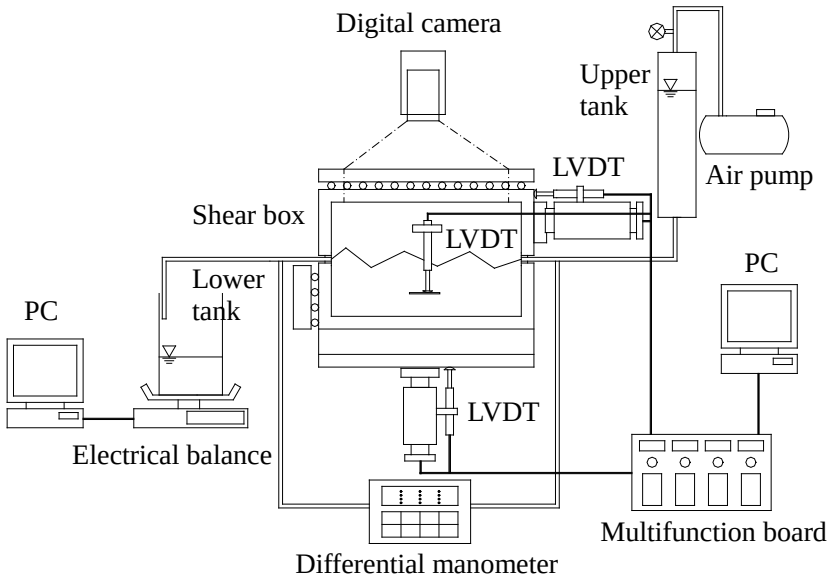

Figure 1. Schematic view of the coupled shear-flow test apparatus, (a) normal and shear load units; (b) hydraulic test mechanism.

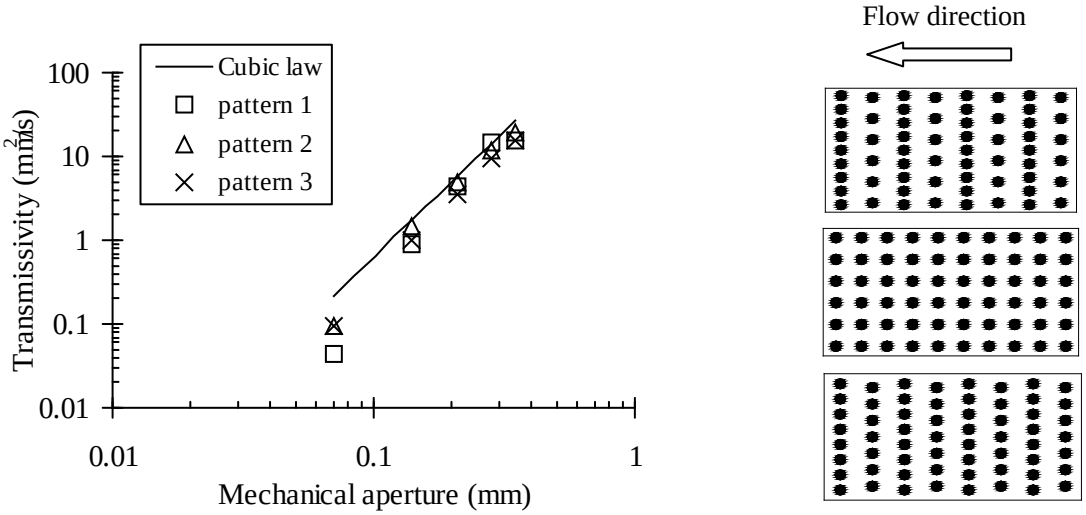

(a) Contact ratio 15%

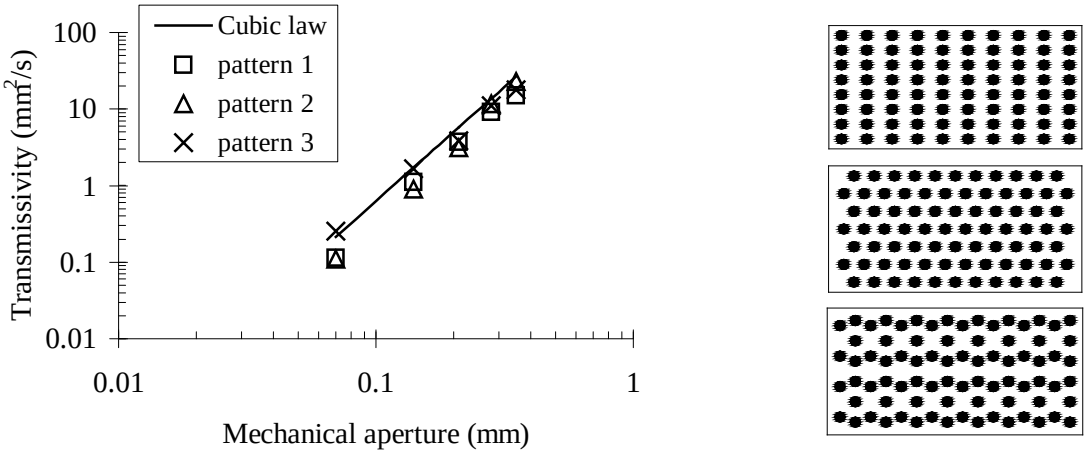

(b) Contact ratio 20%

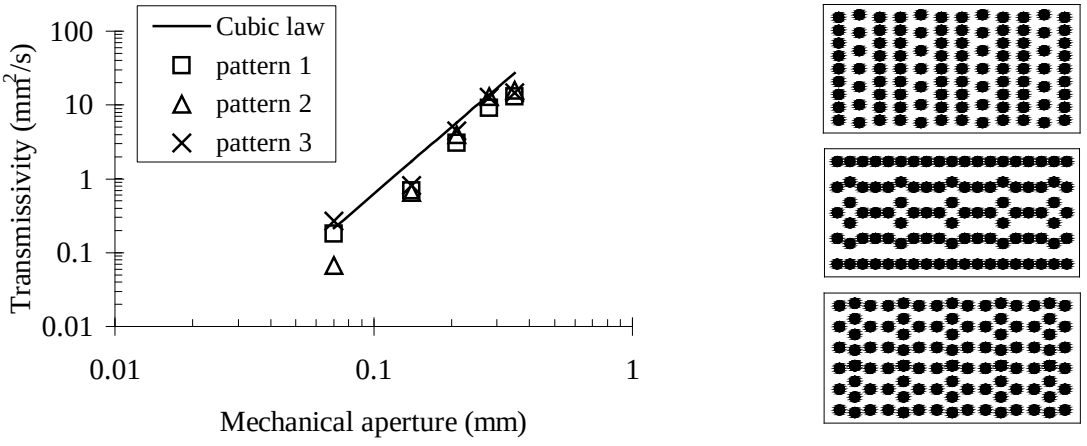

(c) Contact ratio 25%

Figure 2. Transmissivities for three kinds of parallel-plates models with different contact ratios. The distribution patterns at right part of the figure follow the order of pattern 1, pattern 2 and pattern 3, respectively, from top to bottom for each contact ratio.

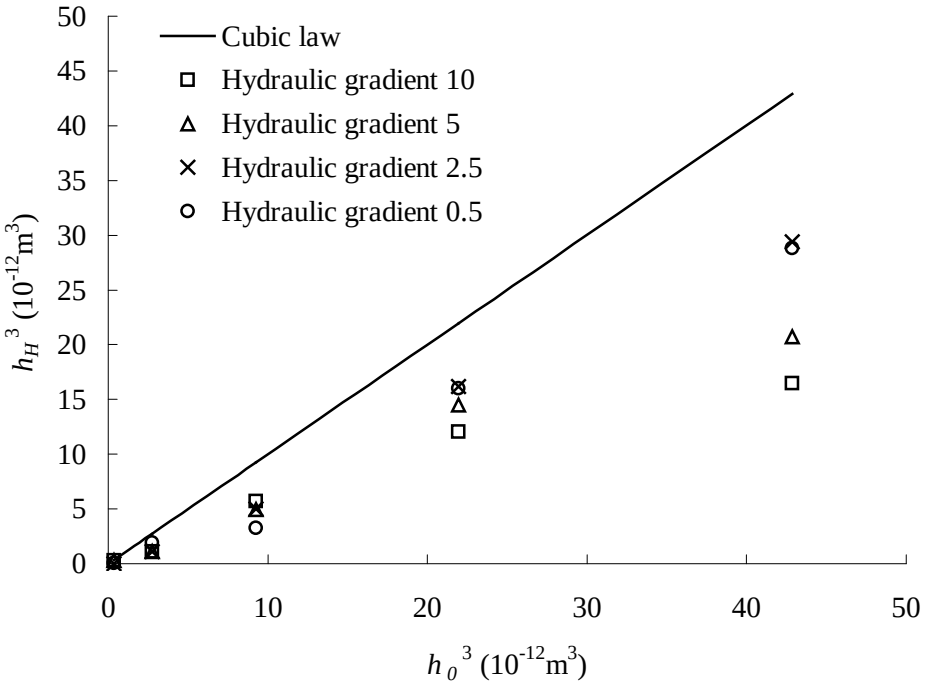

Figure 3. Hydraulic conductance h_H^3 versus the cube of effective hydraulic aperture h_0^3 for contact ratio 0.15. The turbulence may have been generated with high hydraulic gradients.

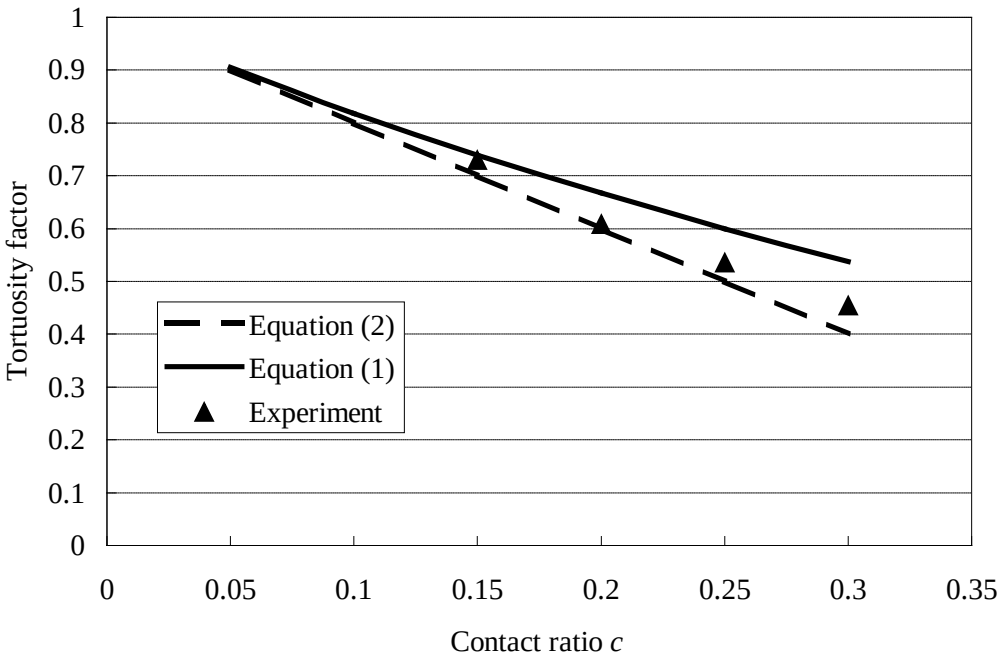

Figure 4. Tortuosity factor versus contact ratio *c*. The tortuosity factors for contact ratios 0.15, 0.2 and 0.25 were taken from the mean values of the three kinds of distributions, respectively. Only one pattern of distribution was tested for contact ratio 0.3. The results from experiment seem to agree more with Equation (2).

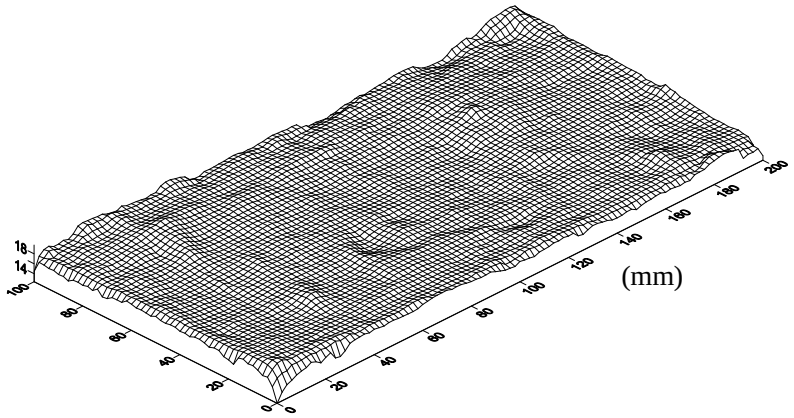

(a) J1

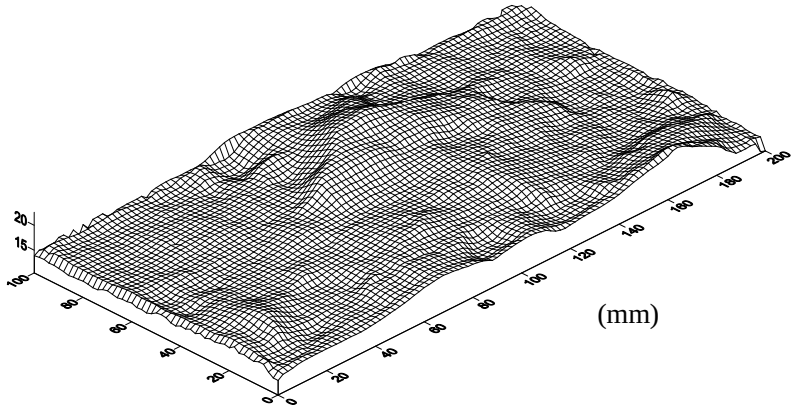

(b) J2

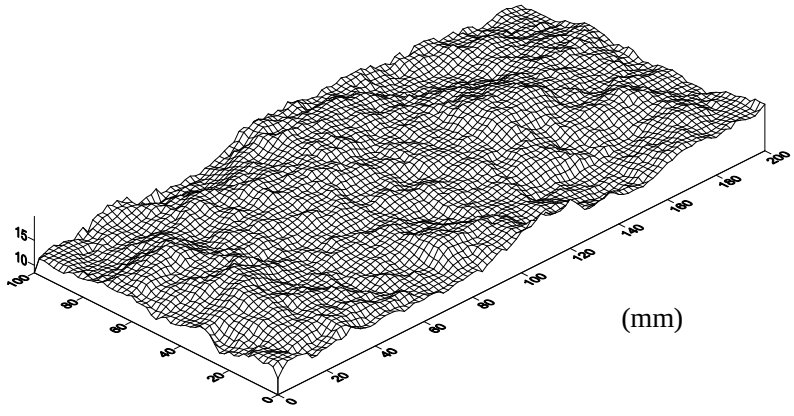

(c) J3

Figure 5. 3-D models of surface topographies of specimen J1, J2 and J3 based on the measured topographical data. J1 has an almost flat surface, the surface of J2 is smooth but a major asperity exists at the center part, J3 is very rough with plenty of small asperities. It should be noted that the size of mesh used in this figure is 2mm different from the one used in measurement 0.2mm.

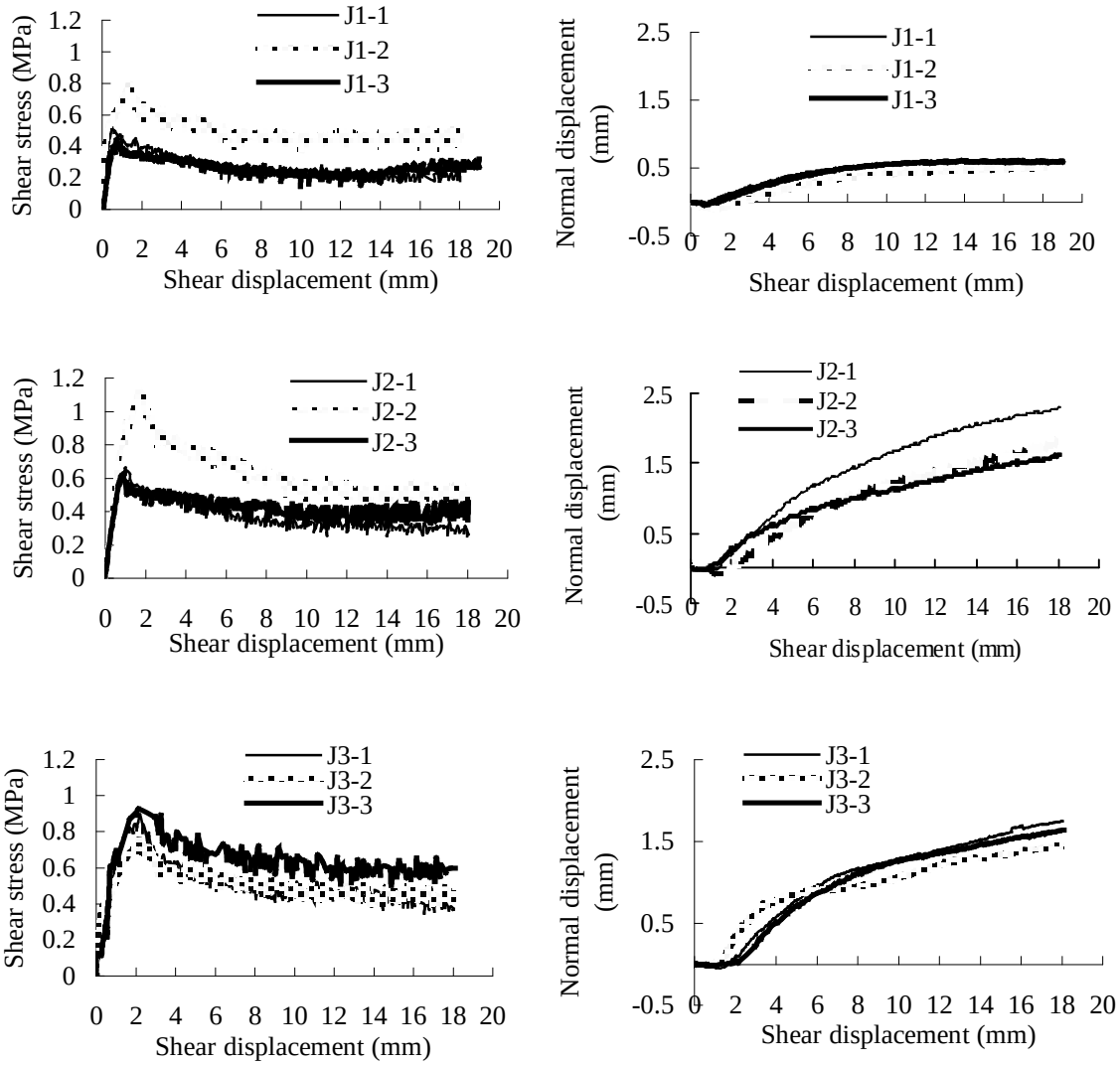

Figure 6. Direct shear test results on specimens J1, J2 and J3. The left three figures show the shear stress versus shear displacement and the right ones are normal displacement versus shear displacement. The test results shown in this figure were directly taken from the recording system of test apparatus without any embellishment. The wobbles in the figures are due to the interaction and destruction of asperities on the upper and lower fracture surafces during shearing. The rougher a fracture surface is, the more obvious the wobbles become.

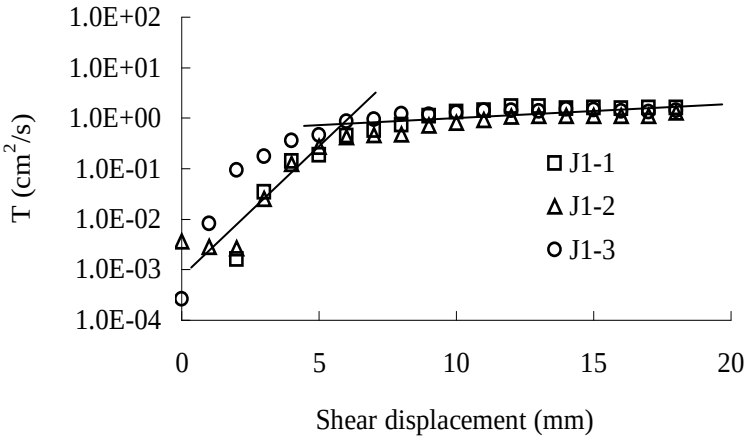

(a) Conductivity of J1

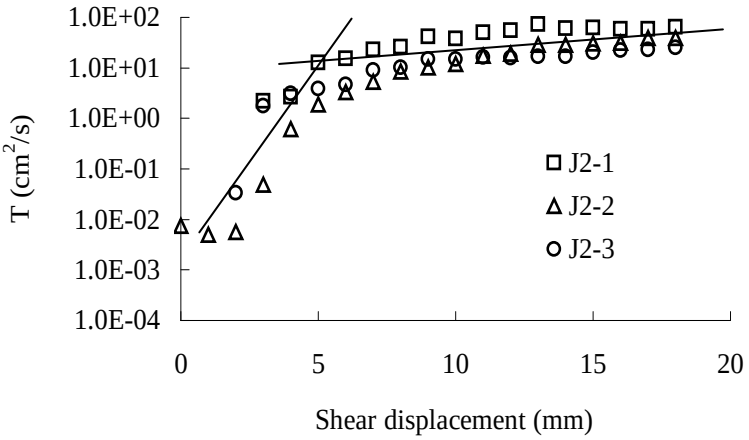

(b) Conductivity of J2

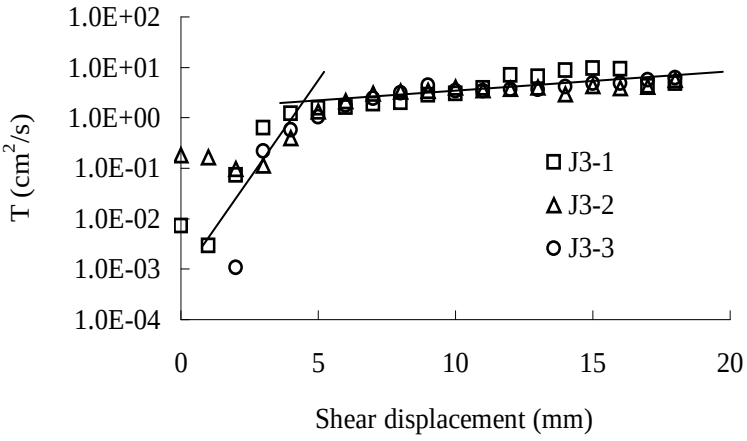

(c) Conductivity of J3

Figure 7. Two-phase behavior of the change of conductivity during shearing. A minus dilation of fracture occurs when a shear starts which causes the decrease of conductivity in phase I . After this, a rapid increase happens till the second phase in which the conductivity trends to keep constant.

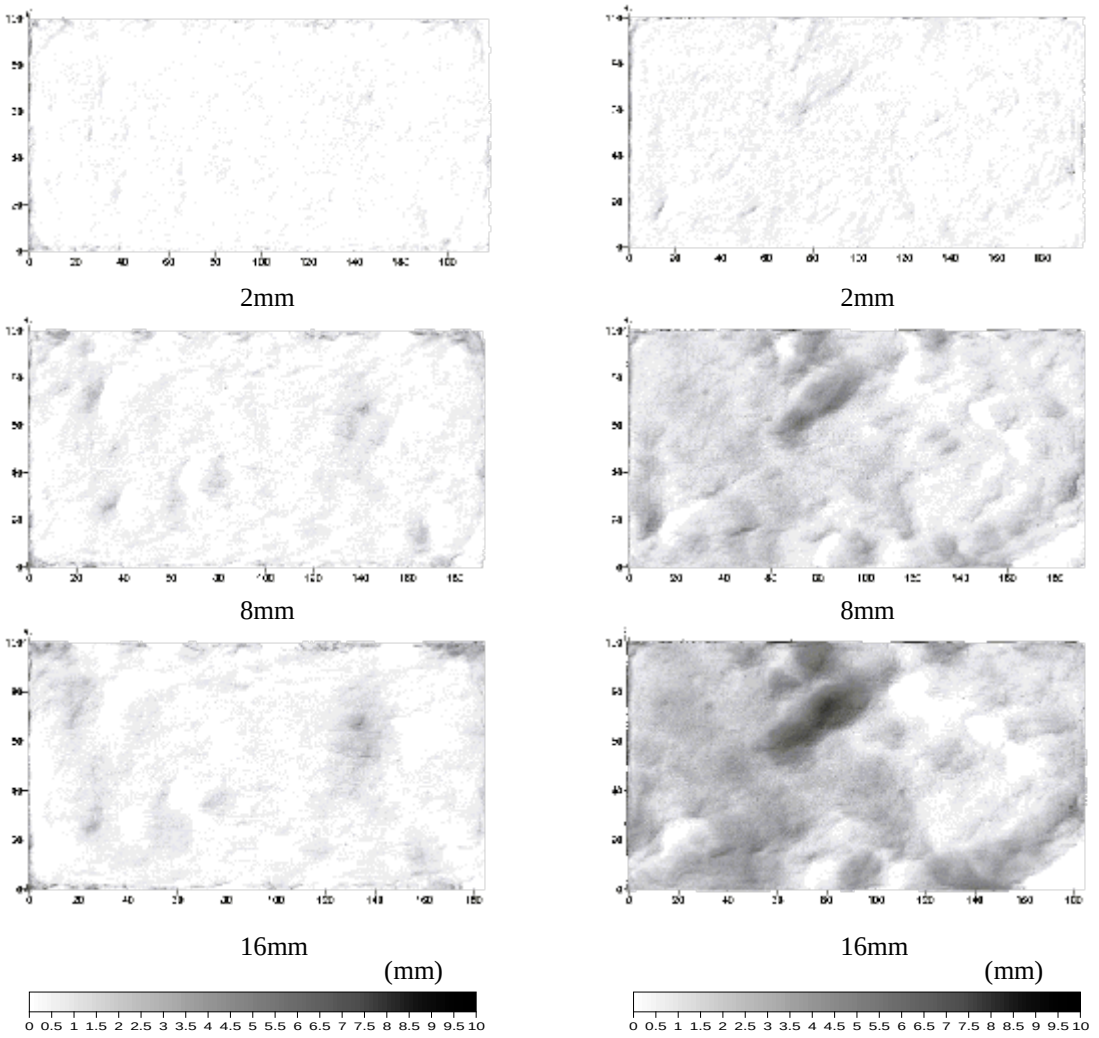
2mm
2mm
8mm
8mm
16mm
16mm
(mm)
(mm)
0 0.5 1 1.5 2 2.5 3 3.5 4 4.5 5 5.5 6 6.5 7 7.5 8 8.5 9 9.5 10
0 0.5 1 1.5 2 2.5 3 3.5 4 4.5 5 5.5 6 6.5 7 7.5 8 8.5 9 9.5 10

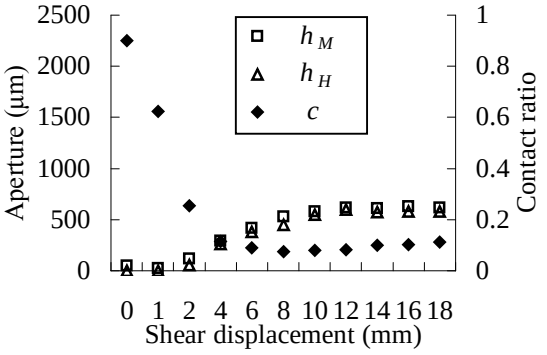
Aperture (μm)
Contact ratio
Shear displacement (mm)
h_M
h_H
c
0 500 1000 1500 2000 2500
0 0.2 0.4 0.6 0.8 1
0 1 2 4 6 8 10 12 14 16 18

(a) J1-1

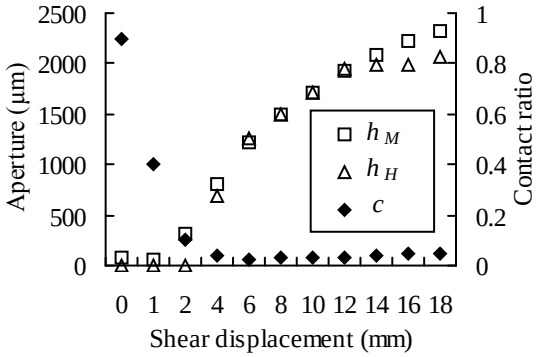
Aperture (μm)
Contact ratio
Shear displacement (mm)
h_M
h_H
c
0 500 1000 1500 2000 2500
0 0.2 0.4 0.6 0.8 1
0 1 2 4 6 8 10 12 14 16 18

(b) J2-1

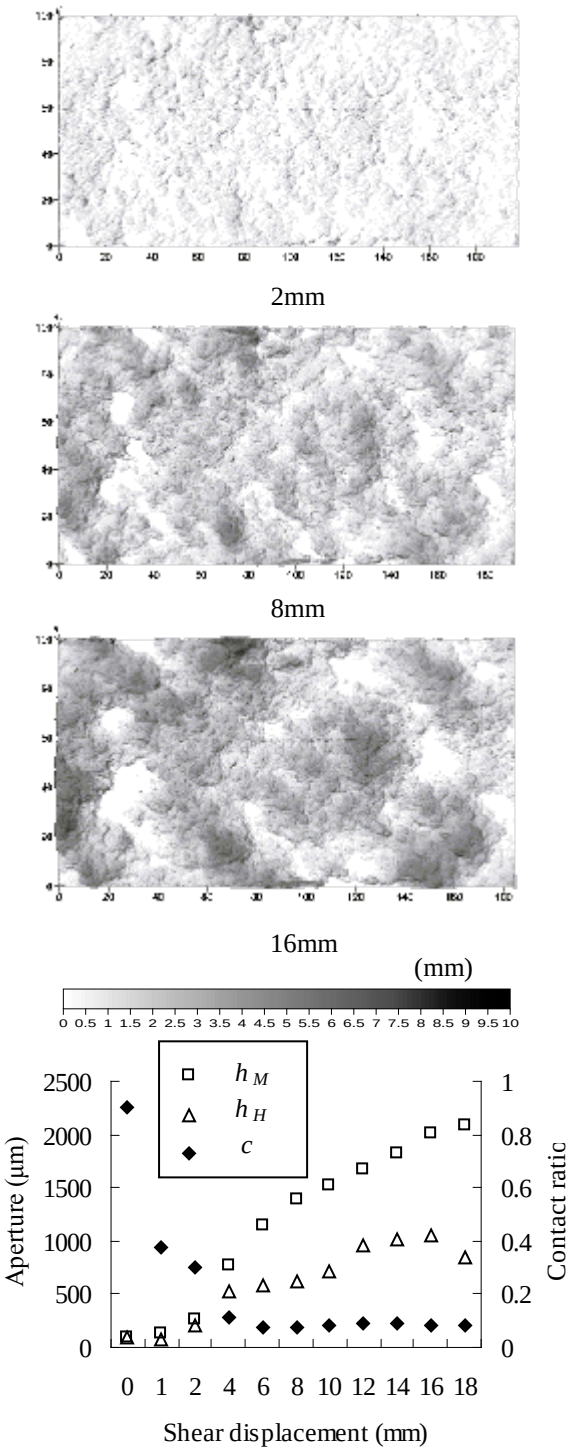

(c) J3-1

Figure 8. Comparison of the change of mechanical aperture h_M, hydraulic aperture h_H and contact ratio c of specimens J1-1, J2-1 and J3-1 during shearing. The upper three figures in figures (a), (b) and (c) show the distributions of mechanical apertures at shear offsets of 2mm, 8mm and 16mm, respectively. The white parts in these figures are the contact areas. The contact ratios at the initial state (0 shear displacement) for each case were assumed to be 0.9 since the fracture specimens were perfectly mated.

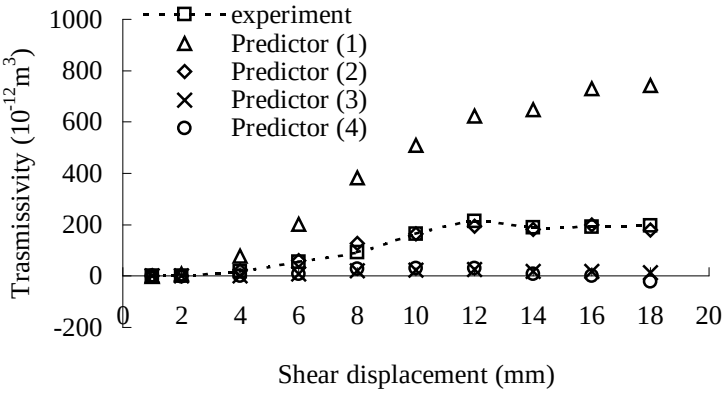

(a) Transmissivity versus shear displacement for J1-1

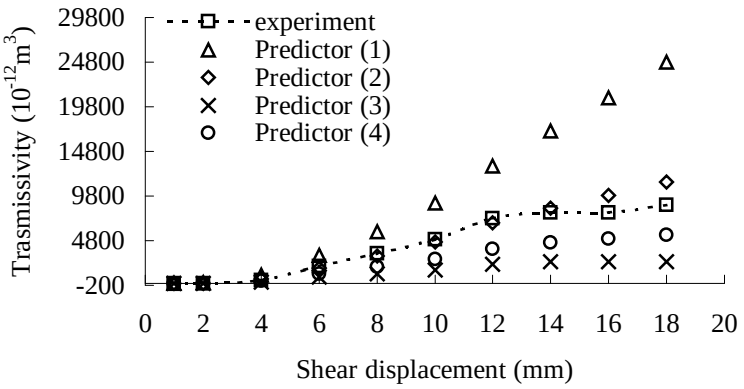

(b) Transmissivity versus shear displacement for J2-1

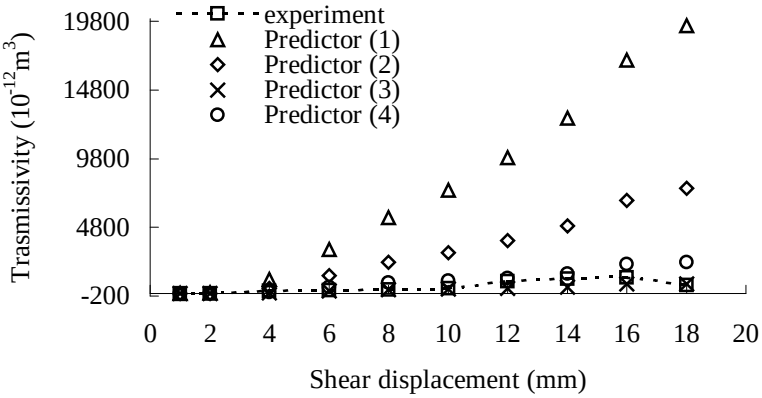

(c) Transmissivity versus shear displacement for J3-1

Predictor (1): $\langle h^3 \rangle (1-2c)$	Predictor (2): $\langle h \rangle^3 (1-2c)$
Predictor (3): $h_G^3 (1-2c)$	Predictor (4): $\langle h \rangle^3 [1-1.5\sigma_h^2 / \langle h \rangle^2](1-2c)$

Figure 9. Comparisons of various predictors to experiment results for test cases J1-1, J2-1 and J3-1. Predictor (3) and (4) are more accurate predictors when a fracture is rough enough to effectively produce complicated void geometry as shown in Figure 8 (c).

Table 1. Physico-mechanical properties of specimen.

Physico-mechanical properties	Index	Unit	Value
Density	ρ	g/cm^3	2.066
Compressive strength	σ_c	MPa	38.5
Modulus of elasticity	E_s	MPa	28700
Poisson's ratio	ν	-	0.23
Tensile strength	σ_t	MPa	2.5
Cohesion	c	MPa	5.3
Internal friction angle	ϕ	°	60

Table 2. Experiment cases under CNL and CNS boundary conditions.

Specimen	Case No.	Roughness (JRC range)	Boundary condition	
			Initial normal stresses δ_n (MPa)	Normal stiffness k_n (GPa/m)
J1	J1-1	0~2	1.0	0
	J1-2		1.5	0
	J1-3		1.0	0.5
J2	J2-1	12~14	1.0	0
	J2-2		2.0	0
	J2-3		1.0	0.5
J3	J3-1	16~18	1.0	0
	J3-2		1.0	0.2
	J3-3		1.0	0.5